

Giant spontaneous magnetostriction in MnTe driven by a novel magnetostructural coupling mechanism

Raju Baral,¹ Milinda Abeykoon,² Branton J. Campbell,¹ and Benjamin A. Frandsen¹

¹*Department of Physics and Astronomy, Brigham Young University, Provo, Utah 84602, USA.*

²*Photon Sciences Division, Brookhaven National Laboratory, Upton, NY, 11973 USA.*

We present a comprehensive x-ray scattering study of spontaneous magnetostriction in hexagonal MnTe, an antiferromagnetic semiconductor with a Néel temperature of $T_N = 307$ K. We observe the largest spontaneous magnetovolume effect known for an antiferromagnet, reaching a volume contraction of $|\Delta V/V| > 7 \times 10^{-3}$. This can be justified semiquantitatively by considering bulk material properties, the spatial dependence of the superexchange interaction, and the geometrical arrangement of magnetic moments in MnTe. The highly unusual *linear* scaling of the magnetovolume effect with the short-range magnetic correlations, beginning in the paramagnetic state well above T_N , points to a novel physical mechanism, which we explain in terms of a trilinear coupling of the elastic strain with superposed distinct domains of the antiferromagnetic order parameter. This novel mechanism for coupling lattice strain to robust short-range magnetic order casts new light on magnetostrictive phenomena and also provides a template by which the exceptional magnetostrictive properties of MnTe might be realized in a wide range of other functional materials.

INTRODUCTION

Despite its simple composition and structure, hexagonal manganese telluride (MnTe; space group $P6_3/mmc$, #194 [1]) exhibits a rich variety of electronic and magnetic behaviors that have sparked a surge of recent interest and have shown promise in numerous technological applications. As an antiferromagnetic (AFM) semiconductor with a Néel temperature of 307 K, MnTe has emerged as a promising platform for AFM spintronics [2–4]. When doped with charge carriers, it demonstrates outstanding thermoelectric properties [5–10], due in large part to the influence of short-range magnetic correlations on the thermopower at high temperature [11–13]. MnTe can also be viewed as a structural component of the intrinsic magnetic topological insulator MnBi_2Te_4 , in which Bi_2Te_3 is intercalated by layers of magnetic MnTe [14], extending the interest in MnTe into the realm of topological quantum materials. More philosophically, MnTe has intrigued researchers as a “crossroads” material for its electronic properties, which are intermediate between strongly correlated insulators like MnO and more weakly correlated metals like MnSb [15, 16].

Yet another promising aspect of MnTe, although one that has received little attention to date, is the magnetostructural behavior associated with the AFM transition. In this work, we explore the phenomenon of magnetostriction, by which the dimensions of a solid change in response to an applied magnetic field (forced magnetostriction) or the development of intrinsic magnetic order (spontaneous magnetostriction). This effect has found widespread application in both established and emerging technologies [17], including sensors, actuators, and transducers [18]; biomedical devices [19]; SONAR [20, 21]; zero- or negative-thermal-expansion materials [22]; and straintronics for energy efficient computing [23], among others. However, a comprehensive understanding of the magnetostrictive effects observed

in many classes of magnetic materials is lacking, particularly for spontaneous magnetostriction [24]. Although studies of magnetostriction have historically focused on ferromagnetic materials, the tremendous diversity of antiferromagnetic phases provides an outstanding opportunity for fundamental investigations of magnetostriction [25], leading to a burgeoning interest in magnetostrictive antiferromagnets [26–30].

Here, we use x-ray scattering to gain detailed insight into the spontaneous magnetostriction in MnTe in response to the AFM transition. We observe a magnetically-driven volume contraction greater than 0.7% in MnTe and Na-doped MnTe, which constitutes the largest known magnetovolume response in an antiferromagnet by a wide margin and is comparable in magnitude to values observed in commercially exploited ferromagnets exhibiting “giant” magnetostriction such as Terfenol-D [21]. The magnetostructural response is initially driven by local magnetic correlations that develop well above the Néel temperature, highlighting the influence of short-range correlations on macroscopic properties. Surprisingly, the lattice contraction scales linearly with the local magnetic order parameter m , in contrast to the typical m^2 dependence that is widely observed in other materials. This linear response points to a previously unknown magnetostrictive mechanism, which we show can be explained by free energy arguments that explicitly consider the coupling of distinct domains of a short-range magnetic order parameter. In addition to revealing the exceptional magnetostructural properties of MnTe, this work provides new insights into fundamental aspects of spontaneous magnetostriction.

EXPERIMENTAL DETAILS

Polycrystalline samples of pure MnTe and 2% Na-doped MnTe were synthesized as described in Ref. 13.

X-ray scattering experiments were performed at beamline 28-ID-1 of the National Synchrotron Light Source II (NSLS-II) at Brookhaven National Laboratory. The samples were loaded into polyimide capillaries and placed in a liquid helium cryostat mounted on the beamline. Temperature-dependent data were collected using a wavelength of 0.19 Å. Additional measurements were performed at selected temperatures with an *in situ* magnetic field using a 5-T magnet mounted on the beamline. The wavelength was 0.106 Å for the field-dependent measurements. The diffraction patterns were azimuthally integrated using DIOPTAS [31] to obtain one-dimensional intensity patterns, which were then normalized and Fourier transformed in XPDFsuite [32] to produce atomic pair distribution function (PDF) data, which is sensitive to both the average and local structure [33]. The maximum momentum transfer included in the Fourier transform was 25 Å^{-1} for the temperature-dependent data and 18 Å^{-1} for the field-dependent data. Structural fits to the data using the published hexagonal crystal structure of MnTe were performed with PDFgui [34] over the real-space range of $1.5 - 50 \text{ Å}$. Representative fits are shown in the Supplementary Information (SI). We performed symmetry analyses of the magnetic order parameters and the invariant free energy polynomial using the ISODISTORT [35, 36] and INVARIANTS [37, 38] programs of the ISOTROPY Software Suite (<https://iso.byu.edu>), respectively.

RESULTS

The hexagonal lattice parameters a and c are shown in Fig. 1 (a) and (b) as a function of temperature as determined from fits to the x-ray PDF data. With decreasing temperature from 500 to $\sim 375 \text{ K}$, the lattice parameters decrease linearly, as expected for conventional thermal contraction. However, upon further cooling toward $T_N \sim 307 \text{ K}$, the lattice parameters decrease at a significantly faster rate, dropping below the trend extrapolated from higher temperature. We observe a similar effect in Na-doped MnTe (see SI). This is clear evidence for spontaneous magnetostriction in MnTe in response to the development of magnetic order.

To probe this behavior more quantitatively, we modeled the expected temperature dependence of the lattice parameters and unit cell volume in the absence of magnetism using the Grüneisen equation of state combined with the Debye approximation of the internal energy. According to this Debye-Grüneisen model, the unit cell volume as a function of temperature T is given by [39, 40]

$$V(T) = \alpha T \left(\frac{T}{T_D} \right)^3 \int_0^{T_D/T} \frac{x^3}{(e^x - 1)} dx + V_0, \quad (1)$$

where $V(T)$ is the temperature-dependent unit cell volume, V_0 is the volume at 0 K, α is given by $9Nk_B\gamma/B_0$, γ is the Grüneisen parameter, $N = 4$ is the number

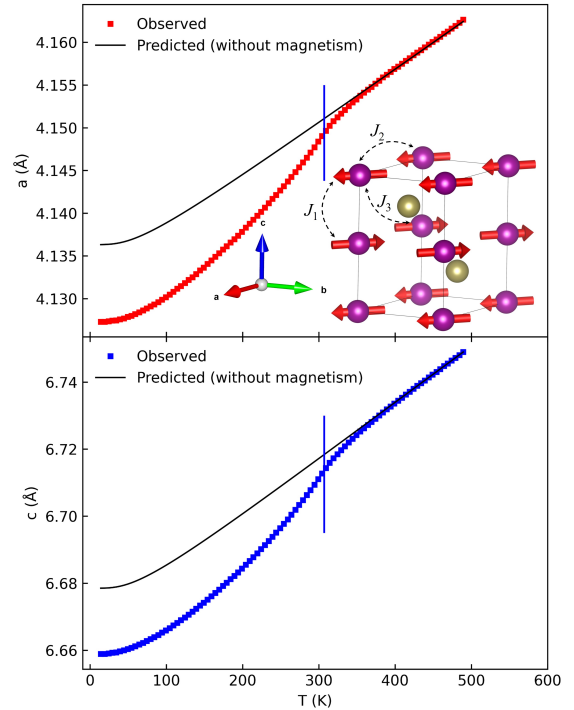


FIG. 1. (a) Temperature dependence of the observed values of a and the prediction based on the Debye-Grüneisen model, which does not include magnetism. Error bars are smaller than the symbol size. Inset: Crystal and magnetic structure of MnTe with the first three magnetic exchange interactions labeled as J_1 , J_2 , and J_3 . Purple (gold) spheres represent Mn (Te) atoms. The red arrows represent the Mn^{2+} magnetic moments. (b) Same as panel (a), but for c .

of atoms per unit cell, B_0 is the bulk modulus at 0 K, and T_D is the Debye temperature, determined by previous experiments to be 223 K [11]. The cubed root of the right hand side of Eq. 1 can be used for the individual lattice parameters a and c [39, 40]. Fitting this model to the lattice parameter and unit cell volume data above 420 K, we can determine values for γ/B_0 and V_0 , which we then use to calculate the full temperature dependence down to 0 K. The best-fit values of γ/B_0 (see SI) are close to the values determined for similar materials such as MnF_2 [39] and consistent with the reported bulk modulus of MnTe [41]. We note that using a wide range of Debye temperatures between 140 K and 300 K makes only a small difference to the fitting results. An equivalent analysis was also performed for the Na-doped sample (see SI).

The calculated lattice parameter trends are shown by the black curves in Fig. 1. These curves represent the expected temperature dependence of the lattice parameters without any magnetic influence; thus, the difference between the observed and predicted lattice parameter values can be attributed to spontaneous magnetostriction associated with the magnetic phase transition. The magnetostriction is quantified as $\Delta\ell/\ell$, where ℓ is the

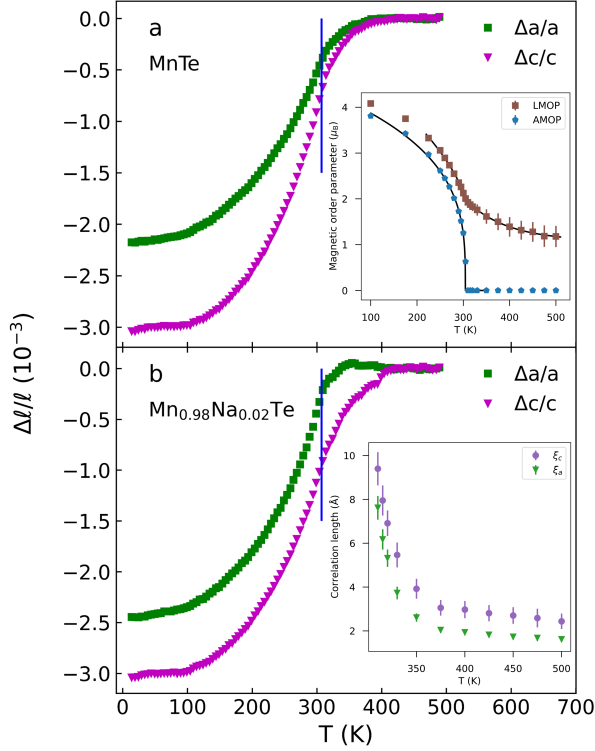


FIG. 2. (a) Spontaneous magnetostriction along the a and c axes in pure MnTe. Inset: Local and average magnetic order parameter (LMOP and AMOP) as a function of temperature. (b) Same as panel (a), but for Na-doped MnTe. Inset: Temperature dependence of the magnetic correlation length along a and c in the paramagnetic state.

observed lattice parameter (either a or c in our case) and $\Delta\ell$ is the observed lattice parameter minus the predicted value. We plot this value as a function of temperature for both the pure and Na-doped samples in Fig. 2. In all cases, $\Delta\ell/\ell$ is close to zero above 400 K, indicating that the calculated lattice parameters accurately capture the high-temperature trend. Between 400 and 350 K, $\Delta\ell/\ell$ begins to trend negative, marking the onset of the spontaneous magnetostriction. This is well above $T_N = 307$ K (marked by the vertical blue lines in Fig. 2), indicating that short-range magnetic correlations in the paramagnetic state initially drive the magnetostriction. To demonstrate this further, we show in the inset to Fig. 2(a) the average magnetic order parameter (AMOP) and the local magnetic order parameter (LMOP) determined from magnetic PDF analysis [42, 43], as recently reported elsewhere [13]. The AMOP corresponds to long-range magnetic order and shows a conventional transition at 307 K, while the LMOP corresponds to nearest-neighbor magnetic correlations and persists deep into the paramagnetic phase. The inset to Fig. 2(b) shows the thermal evolution of the in-plane and out-of-plane correlation lengths (ξ_a and ξ_c , respectively), which exhibit a strong increase as the temperature is lowered below ~ 350 K, coinciding with the

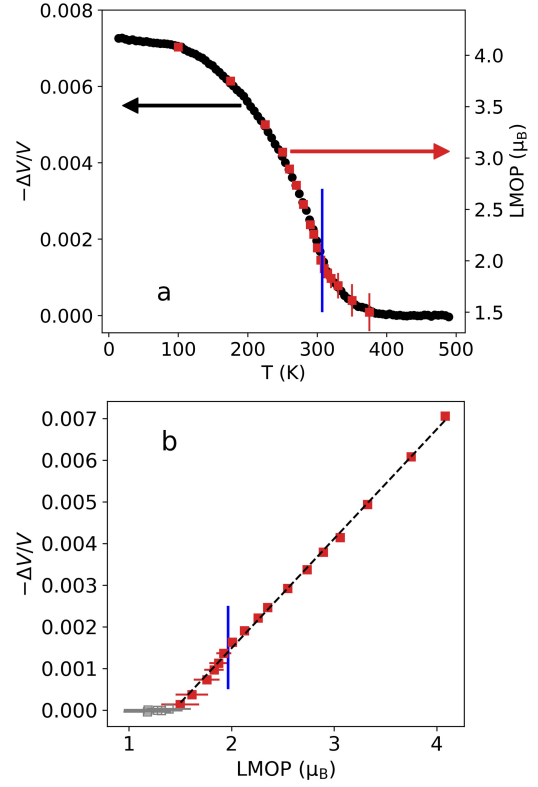


FIG. 3. (a) Temperature dependence of the magnitude of the magnetovolume shift in MnTe (black symbols, left vertical axis) and the local magnetic order parameter (red symbols, right vertical axis). T_N is marked by the blue vertical line. (b) Magnetovolume shift versus local magnetic order parameter, showing a linear correlation. The blue line marks the long-range ordering transition; points to the left (right) of the line are in the paramagnetic (long-range AFM) state. The dashed line is the best-fit line to the data points shown by red symbols. The gray data points were excluded because they correspond to high temperatures above the onset of the magnetostructural response.

onset of the magnetostructural response. This is further evidence that the local magnetic correlations in the paramagnetic state drive the spontaneous magnetostriction when the correlation length is sufficiently large. These observations provide useful insights into models of magnetostructural coupling when short-range magnetic correlations are present. We expect this coupling between the long-range crystal structure and short-range magnetic correlations to be relevant to numerous other magnetic materials that have a correlated paramagnetic state.

Fig. 3(a) displays the relative volume change, $-\Delta V/V$, in black symbols, with the minus sign included for convenience to produce an overall positive quantity. Upon cooling, the magnetovolume shift begins to deviate from zero slightly below 400 K. At the lowest measured temperature, $\Delta V/V = -7.3 \times 10^{-3}$ for pure MnTe and -7.8×10^{-3} for Na-doped MnTe (see the SI). To our knowledge, this is the largest spontaneous magnetovol-

ume effect reported for any antiferromagnetic material to date and is several times larger than that observed in model antiferromagnets like CrF_2 (-7.72×10^{-4}), CuF_2 (-1.16×10^{-4}) [40], MnF_2 (-1×10^{-3}), and NiF_2 (-4.5×10^{-4}) [39]. Even for ferromagnetic materials, this would be a large magnetovolume effect, reaching a magnitude similar to that observed in commercial magnetostrictive materials like Terfenol-D [21]. At the same time, MnTe exhibits no observable forced magnetostriction in fields up to 5 T (see the SI), which is unsurprising for an antiferromagnet.

We explore the nature of the magnetostructural coupling in more detail by comparing the magnetic order parameter to the spontaneous magnetovolume shift. The LMOP is plotted as a function of temperature on the right vertical axis in Fig. 3(a), where we see that the LMOP data points below 400 K fall directly on the magnetovolume curve (left vertical axis) for the selected axis scaling. This reveals a striking direct proportionality between the LMOP and the magnetostriction, as demonstrated in Fig. 3(b). A linear relationship is evident from the lowest temperature measured (100 K; upper right corner of the plot) up to about 400 K (lower left region of the plot). Above 400 K, the magnetovolume shift goes to zero while the LMOP persists. The Na-doped sample also exhibits this linear coupling, as shown in the SI. We conclude that in both the paramagnetic and antiferromagnetic phases, the magnetovolume shifts in both pure and Na-doped MnTe are linearly proportional to the LMOP, which gradually evolves into the AMOP below T_N .

DISCUSSION

The magnitude of a magnetostrictive response is determined by the balance between elastic energy costs and magnetic energy savings caused by changing the interatomic distances. In MnTe, the magnetic interactions are predominantly due to superexchange, with a smaller contribution from direct exchange [44]. In either case, the interactions depend strongly on the relative positions of ions. The interactions between the first three nearest neighbors (see inset to Fig. 1) are $J_1 = -21.5$ K (along c), $J_2 = 0.67$ K (in the ab plane), and $J_3 = -2.87$ K (diagonally out of the plane) [45]. In superexchange systems where a single interaction along one crystalline axis dominates (as is the case with J_1 here), a simple energy minimization argument leads to the relation [46]

$$\epsilon_n = \frac{d_0}{VE} \frac{dJ}{dn} \langle \mathbf{S}_i \cdot \mathbf{S}_j \rangle, \quad (2)$$

where ϵ_n is the strain along a given direction \hat{n} , n is the coordinate along \hat{n} , d_0 is the equilibrium distance between neighboring magnetic ions in the absence of magnetism, V is the unit cell volume, E is the Young's modulus along \hat{n} , and J is the magnetic interaction between

the neighboring magnetic moments \mathbf{S}_i and \mathbf{S}_j . Based on this equation, we can estimate the expected strain along the c axis for MnTe. We know the values of d_0 and V from the present work; the bulk modulus of MnTe has previously been reported as 47.3 GPa [41], which we use for E ; and we can estimate dJ/dn to be -5×10^{-12} J/m based on tabulated superexchange interactions at various distances with similar cation-anion-cation angles as observed in MnTe [45]. Assuming fully ordered $S = 5/2$ spins, the result is $\epsilon_c \sim 0.002$, which is remarkably close to the observed value of ~ 0.003 at low temperature. Thus, we can attribute the exceptionally large magnetostriction along c to a high density of large magnetic moments, a relatively low bulk modulus, and a strong spatial dependence of J_1 .

Often, a compressive strain along one direction will be partially counteracted by a tensile strain in other dimensions, minimizing the overall volume change. This has been observed, for example, in antiferromagnetic MnO [47] and FeTiO_3 [26] and in various ferromagnetic magnetocalorics [48]. In MnTe, however, both a and c contract significantly as the magnetic correlations develop. We attribute this to the cooperative nature of the exchange interactions, such that no geometrical frustration is present to cause competing magnetoelastic tendencies. The favorable combination of material parameters leading to strong magnetostriction and the geometrical factors promoting the contraction of both a and c are therefore responsible for the exceptionally large magnetovolume effect in MnTe.

A more challenging issue is the clearly linear dependence of the lattice strain on the LMOP in MnTe, which stands in stark contrast to the expected quadratic dependence of strain on the AMOP [28, 39, 40, 49–52]. This quadratic dependence originates from the time-reversal invariance of the free energy, which admits only even combined powers of any magnetic order parameters in the absence of an external magnetic field. We found the solution to this conundrum in the trilinear couplings of elastic strain with two distinct domains of the magnetic order parameter.

The AFM structure of MnTe consists of alternating ferromagnetic layers of in-plane moments oriented between the in-plane lattice basis vectors, so that moments in the $z = 0$ and $z = 0.5$ layers have opposite directions [2, 13, 53]. The magnetic order parameter belongs to irreducible representation (irrep) and order parameter direction (OPD) $\Gamma_5^+(0, a)$ of non-magnetic parent space-group $P6_3/mmc$ (#194), which yields magnetic space group $Cm'c'm$ (BNS 63.462). This magnetic order parameter has six distinct but symmetry-equivalent domains characterized by the moment direction in the $z = 0$ layer, as shown in Fig. 4(a). In this context, short-range magnetic order can be viewed as a dynamically fluctuating spatial distribution of small regions, each possessing one of the domains of the order parameter. Below T_N , one of these six domains emerges as

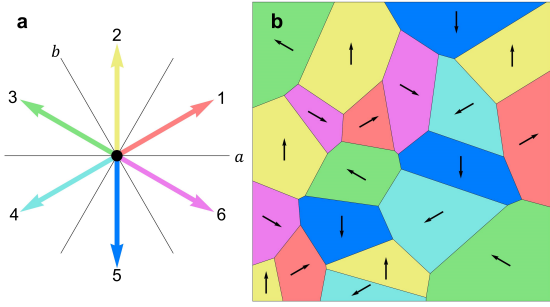


FIG. 4. (a) The $z = 0$ moment direction of each of the six magnetic domains of MnTe is indicated by a colored arrow. The directions marked a and b indicate the hexagonal lattice basis vectors. (b) Schematic representation of short-range-ordered magnetic correlations in the paramagnetic state of MnTe, where the $z = 0$ moment direction indicated by the black arrow within a region of a given color matches the magnetic domain with an arrow of the same color in (a). The magnetic-domain pattern is intended to represent dynamic rather than static short-range magnetic correlations.

the long-range order parameter, while the other domains gradually cease to be represented. We define m_S to be the short-range magnetic order parameter corresponding to any one of the six magnetic domains and m_L to be the emerging long-range magnetic order parameter, which we will arbitrarily associate with domain #1 in Fig. 4(a). Referring to the insets in Fig. 1, we associate m_S with the approximately temperature-independent correlations of magnitude $\sim 1 \mu_B$ and correlation length $\sim 3 \text{ \AA}$ observed above 375 K, while the onset of m_L is identified by the rapid rise in correlation length below 375 K, leading to genuine long-range order below T_N .

As the length scale and lifetime of m_L increase upon cooling toward T_N , the superposition of m_L and m_S becomes important. Each combination of a strain variable ϵ with a domain S of the short-range magnetic order parameter contributes a symmetry-allowed trilinear coupling term of the form $\epsilon m_L m_S$ to the free energy, where the coefficient of the term depends on the angle between the orientations of their $z = 0$ moment directions from Fig. 4(a). Minimizing the free energy, which also includes an ϵ^2 term, with respect to strain then yields $\epsilon \sim m_L m_S$. The key observation is that the LMOP (m_S) is already large and relatively temperature insensitive when the magnetostriction begins around 375 K, so that it can be treated as a *pre-existing* order parameter. This provides a symmetry-allowed mechanism through which ϵ can track linearly with m_L , thus leading to the observed linear magnetostrictive response. This reasoning also applies to the magnetic structure of Na-doped MnTe, as demonstrated in the SI.

To our knowledge, linear spontaneous magnetostriction has not been reported previously, making MnTe unique both for the exceptionally large magnitude and the linear nature of the spontaneous magnetostriction.

However, we expect that other materials with a correlated paramagnetic state and suitable domain couplings may also exhibit such behavior, making this perhaps a more widespread mechanism for spontaneous magnetostriction. This work also motivates further study of the oft-overlooked role of short-range magnetic order in magnetostructural effects and the coupling of domains of short-range order parameters in general.

Acknowledgements

We thank Chris Howard for helpful discussions regarding magnetostructural coupling. B.A.F. and R.B. were supported by the U.S. Department of Energy, Office of Science, Basic Energy Science through Award No. DE-SC0021134. This research used beamline 28-ID-1 of the National Synchrotron Light Source II, a U.S. Department of Energy (DOE) Office of Science User Facility operated for the DOE Office of Science by Brookhaven National Laboratory under Contract No. DE-SC0012704.

Conflict of Interest

The authors declare no conflict of interest.

-
- [1] W. D. Johnston and D. E. Sestrich, The MnTe-GeTe phase diagram, *J. Inorg. Nucl. Chem.* **19**, 229 (1961).
 - [2] D. Kriegner, K. Výborný, K. Olejník, H. Reichlová, V. Novák, X. Marti, J. Gazquez, V. Saidl, P. Němec, V. V. Volobuev, G. Springholz, V. Holý, and T. Jungwirth, Multiple-stable anisotropic magnetoresistance memory in antiferromagnetic MnTe, *Nat. Commun.* **7**, 11623 (2016).
 - [3] G. Yin, J.-X. Yu, Y. Liu, R. K. Lake, J. Zang, and K. L. Wang, Planar Hall Effect in Antiferromagnetic MnTe Thin Films, *Phys. Rev. Lett.* **122**, 106602 (2019).
 - [4] D. Bossini, S. Dal Conte, M. Terschanski, G. Springholz, A. Bonanni, K. Deltenre, F. Anders, G. S. Uhrig, G. Cerullo, and M. Cinchetti, Femtosecond phononic coupling to both spins and charges in a room-temperature antiferromagnetic semiconductor, *Phys. Rev. B* **104**, 224424 (2021).
 - [5] Y. Xu, W. Li, C. Wang, J. Li, Z. Chen, S. Lin, Y. Chen, and Y. Pei, Performance optimization and single parabolic band behavior of thermoelectric MnTe, *J. Mater. Chem. A* **5**, 19143 (2017).
 - [6] Y. Ren, J. Yang, Q. Jiang, D. Zhang, Z. Zhou, X. Li, J. Xin, and X. He, Synergistic effect by Na doping and S substitution for high thermoelectric performance of p-type MnTe, *J. Mater. Chem. C* **5**, 5076 (2017).
 - [7] J. Dong, C.-F. Wu, J. Pei, F.-H. Sun, Y. Pan, B.-P. Zhang, H. Tang, and J.-F. Li, Lead-free MnTe mid-temperature thermoelectric materials: facile synthesis, p-type doping and transport properties, *J. Mater. Chem. C* **6**, 4265 (2018).
 - [8] H. Deng, X. Lou, W. Lu, J. Zhang, D. Li, S. Li, Q. Zhang, X. Zhang, X. Chen, D. Zhang, Y. Zhang, and G. Tang, High-performance eco-friendly MnTe thermoelectrics through introducing SnTe nanocrystals and manipulating band structure, *Nano Energy* **81**, 105649 (2021).
 - [9] W. Xiong, Z. Wang, X. Zhang, C. Wang, L. Yin, Y. Gong, Q. Zhang, S. Li, Q. Liu, P. Wang, Y. Zhang,

- and G. Tang, Lattice Distortions and Multiple Valence Band Convergence Contributing to High Thermoelectric Performance in MnTe, *Small* **19**, 2206058 (2023).
- [10] S. Zulkifal, Z. Wang, X. Zhang, S. Siddique, Y. Yu, C. Wang, Y. Gong, S. Li, D. Li, Y. Zhang, P. Wang, and G. Tang, Multiple valence bands convergence and localized lattice engineering lead to superhigh thermoelectric figure of merit in mnTe, *Adv. Sci.*, 2206342 (2023).
 - [11] Y. Zheng, T. Lu, M. M. H. Polash, M. Rasoulianboroujeni, N. Liu, M. E. Manley, Y. Deng, P. J. Sun, X. L. Chen, R. P. Hermann, D. Vashaee, J. P. Heremans, and H. Zhao, Paramagnon drag in high thermoelectric figure of merit Li-doped MnTe, *Sci. Adv.* **5**, eaat9461 (2019).
 - [12] M. M. H. Polash, D. Moseley, J. Zhang, R. P. Hermann, and D. Vashaee, Understanding and design of spin-driven thermoelectrics, *Cell Rep. Phys. Sci.* **2**, 100614 (2021).
 - [13] R. Baral, J. Christensen, P. Hamilton, F. Ye, K. Chesnel, T. D. Sparks, R. Ward, J. Yan, M. A. McGuire, M. E. Manley, J. B. Staunton, R. P. Hermann, and B. A. Frandsen, Real-space visualization of short-range antiferromagnetic correlations in a magnetically enhanced thermoelectric, *Matter* **5**, 1853 (2022).
 - [14] Y. Deng, Y. Yu, M. Z. Shi, Z. Guo, Z. Xu, J. Wang, X. H. Chen, and Y. Zhang, Quantum anomalous Hall effect in intrinsic magnetic topological insulator MnBi_2Te_4 , *Science* **367**, 895 (2020).
 - [15] J. W. Allen, G. Lucovsky, and J. C. Mikkelsen Jr., Optical Properties and Electronic Structure of Crossroads Material MnTe, *Solid State Commun.* **24**, 367 (1977).
 - [16] S. J. Youn, B. I. Min, and A. J. Freeman, Crossroads electronic structure of MnS, MnSe, and MnTe, *Phys. Status Solidi B* **241**, 1411 (2004).
 - [17] E. Du Trémolet de Lacheisserie, *Magnetostriction: theory and applications of magnetoelasticity* (CRC Press, Boca Raton, 1993).
 - [18] E. Hristoforou and A. Ktena, Magnetostriction and magnetostrictive materials for sensing applications, *J. Magn. Magn. Mater.* **316**, 372 (2007), proceedings of the Joint European Magnetic Symposia.
 - [19] C. Gao, Z. Zeng, S. Peng, and C. Shuai, Magnetostrictive alloys: Promising materials for biomedical applications, *Bioactive Materials* **8**, 177 (2022).
 - [20] H. Angus and E. Neppiras, Nickel-based magnetostrictive alloys for electromechanical transducers, *Ultrasonics* **7**, 182 (1969).
 - [21] D. Jiles, The development of highly magnetostrictive rare earth-iron alloys, *J. Phys. D: Appl. Phys.* **27**, 1 (1994).
 - [22] Y. Song, N. Shi, S. Deng, X. Xing, and J. Chen, Negative thermal expansion in magnetic materials, *Prog. Mater. Sci.* **121**, 100835 (2021).
 - [23] S. Bandyopadhyay, J. Atulasimha, and A. Barman, Magnetic straintronics: Manipulating the magnetization of magnetostrictive nanomagnets with strain for energy-efficient applications, *Appl. Phys. Rev.* **8**, 041323 (2021), <https://doi.org/10.1063/5.0062993>.
 - [24] D. Sander, Magnetostriction and Magnetoelasticity, in *Handbook of Magnetism and Magnetic Materials*, edited by M. Coey and S. Parkin (Springer International Publishing, Cham, 2020) pp. 1–45.
 - [25] M. Doerr, M. Rotter, and A. Lindbaum, Magnetostriction in rare-earth based antiferromagnets, *Adv. Phys.* **54**, 1 (2005).
 - [26] M. Charilaou, D. Sheptyakov, J. F. Löffler, and A. U. Gehring, Large spontaneous magnetostriction in FeTiO_3 and adjustable magnetic configuration in Fe(III)-doped FeTiO_3 , *Phys. Rev. B* **86**, 024439 (2012).
 - [27] H. K. Singh, I. Samathrakris, N. M. Fortunato, J. Zemen, C. Shen, O. Gutfleisch, and H. Zhang, Multifunctional antiperovskites driven by strong magnetostructural coupling, *npj Comput. Mater.* **7**, 1 (2021).
 - [28] P. Miao, Z. Tan, S. Lee, Y. Ishikawa, S. Torii, M. Yonemura, A. Koda, K. Komatsu, S. Machida, A. Sano-Furukawa, T. Hattori, X. Lin, K. Li, T. Mochiku, R. Kikuchi, C. Kawashima, H. Takahashi, Q. Huang, S. Itoh, R. Kadono, Y. Wang, F. Pan, K. Yamauchi, and T. Kamiyama, Origin of magnetovolume effect in a cobaltite, *Phys. Rev. B* **103**, 094302 (2021).
 - [29] L. Casillas-Trujillo, R. Armiento, and B. Alling, Identification of materials with strong magnetostructural coupling using computational high-throughput screening, *Phys. Rev. Materials* **5**, 034417 (2021).
 - [30] K. Dey, S. Sauerland, B. Ouladdiaf, K. Beauvois, H. Wadepohl, and R. Klingeler, Magnetostructural coupling in ilmenite-type NiTiO_3 , *Phys. Rev. B* **103**, 134438 (2021).
 - [31] C. Prescher and V. B. Prakapenka, DIOPTAS: a program for reduction of two-dimensional X-ray diffraction data and data exploration, *High Pressure Res.* **35**, 223 (2015).
 - [32] X. Yang, P. Juhás, C. Farrow, and S. J. L. Billinge, xPDFsuite: an end-to-end software solution for high throughput pair distribution function transformation, visualization and analysis, *arXiv* (2015), 1402.3163.
 - [33] T. Egami and S. J. L. Billinge, *Underneath the Bragg peaks: structural analysis of complex materials*, 2nd ed. (Elsevier, Amsterdam, 2012).
 - [34] C. L. Farrow, P. Juhás, J. Liu, D. Bryndin, E. S. Božin, J. Bloch, T. Proffen, and S. J. L. Billinge, PDFfit2 and PDFgui: Computer programs for studying nanostructure in crystals, *J. Phys.: Condens. Mat.* **19**, 335219 (2007).
 - [35] B. Campbell, H. Stokes, D. Tanner, and D. Hatch, ISODISPLACE: An Internet Tool for Exploring Structural Distortions, *J. Appl. Crystallogr.* **39**, 607 (2006).
 - [36] H. T. Stokes, D. M. Hatch, and B. J. Campbell, ISODIS-TORT, ISOTROPY Software Suite (2023).
 - [37] D. M. Hatch and H. T. Stokes, INVARIANTS: program for obtaining a list of invariant polynomials of the order-parameter components associated with irreducible representations of a space group, *J. Appl. Crystallogr.* **36**, 951 (2003).
 - [38] H. T. Stokes, D. M. Hatch, and B. J. Campbell, ISODIS-TORT, ISOTROPY Software Suite (2023).
 - [39] T. Chatterji, G. N. Iles, B. Ouladdiaf, and T. C. Hansen, Magnetoelastic effect in MF_2 ($M = \text{Mn}, \text{Fe}, \text{Ni}$) investigated by neutron powder diffraction, *J. Phys.: Condens. Mat.* **22**, 316001 (2010).
 - [40] T. Chatterji and T. C. Hansen, Magnetoelastic effects in Jahn–Teller distorted CrF_2 and CuF_2 studied by neutron powder diffraction, *J. Phys.: Condens. Mat.* **23**, 276007 (2011).
 - [41] W. Paszkowicz and E. Dynowska, HIGH PRESSURE - HIGH TEMPERATURE DIFFRACTION STUDY OF MnTe USING SYNCHROTRON RADIATION, *Acta Phys. Pol. A* **91**, 939 (1997).
 - [42] B. A. Frandsen, X. Yang, and S. J. L. Billinge, Magnetic pair distribution function analysis of local magnetic correlations, *Acta Crystallogr. A* **70**, 3 (2014).

- [43] B. A. Frandsen and S. J. L. Billinge, Magnetic structure determination from the magnetic pair distribution function (mPDF): ground state of MnO, *Acta Crystallogr. A* **71**, 325 (2015).
- [44] S. Mu, R. P. Hermann, S. Gorsse, H. Zhao, M. E. Manley, R. S. Fishman, and L. Lindsay, Phonons, magnons, and lattice thermal transport in antiferromagnetic semiconductor MnTe, *Phys. Rev. Materials* **3**, 025403 (2019).
- [45] W. Szuszkiewicz, E. Dynowska, B. Witkowska, and B. Hennion, Spin-wave measurements on hexagonal MnTe NiAs-type structure by inelastic neutron scattering, *Phys. Rev. B* **73**, 104403 (2006).
- [46] V. S. Zapf, V. F. Correa, P. Sengupta, C. D. Batista, M. Tsukamoto, N. Kawashima, P. Egan, C. Pantea, A. Migliori, J. B. Betts, M. Jaime, and A. Paduan-Filho, Direct measurement of spin correlations using magnetostriiction, *Phys. Rev. B* **77**, 020404 (2008).
- [47] D. Bloch and R. Maury, Uniaxial Stress Experiments and Magnetoelastic Interactions in Manganese Oxide, *Phys. Rev. B* **7**, 4883 (1973).
- [48] Y. M. Oey, J. D. Bocarsly, D. Mann, E. E. Levin, M. Shatruk, and R. Seshadri, Structural changes upon magnetic ordering in magnetocaloric AlFe_2B_2 , *Appl. Phys. Lett.* **116**, 212403 (2020), <https://doi.org/10.1063/5.0007266>.
- [49] H. Pascard and A. Globus, Exchange striction and crystal lattice in domains and domain walls, *J. Appl. Phys.* **53**, 2425 (1982), <https://doi.org/10.1063/1.330833>.
- [50] M. A. Carpenter, Z. Zhang, and C. J. Howard, A linear-quadratic order parameter coupling model for magnetoelectric phase transitions in Fe_{1-x}O and MnO, *J. Phys.: Condens. Mat.* **24**, 156002 (2012).
- [51] T. Chatterji, B. Ouladdiaf, P. F. Henry, and D. Bhattacharya, Magnetoelastic effects in multiferroic YMnO_3 , *J. Phys.: Condens. Mat.* **24**, 336003 (2012).
- [52] L. Oravova, Z. Zhang, N. Church, R. J. Harrison, C. J. Howard, and M. A. Carpenter, Elastic and anelastic relaxations accompanying magnetic ordering and spin-flop transitions in hematite, Fe_2O_3 , *J. Phys.: Condens. Mat.* **25**, 116006 (2013).
- [53] D. H. Moseley, K. M. Taddei, J. Yan, M. A. McGuire, S. Calder, M. M. H. Polash, D. Vashae, X. Zhang, H. Zhao, D. S. Parker, R. S. Fishman, and R. P. Hermann, Giant doping response of magnetic anisotropy in MnTe, *Phys. Rev. Materials* **6**, 014404 (2022).

Supplemental Information: Giant spontaneous magnetostriction in MnTe driven by a novel magnetostructural coupling mechanism

Raju Baral,¹ Milinda Abeykoon,² Branton J. Campbell,¹ and Benjamin A. Frandsen¹

¹*Department of Physics and Astronomy,*

Brigham Young University, Provo, Utah 84602, USA.

²*Photon Sciences Division, Brookhaven National Laboratory, Upton, NY, 11973 USA.*

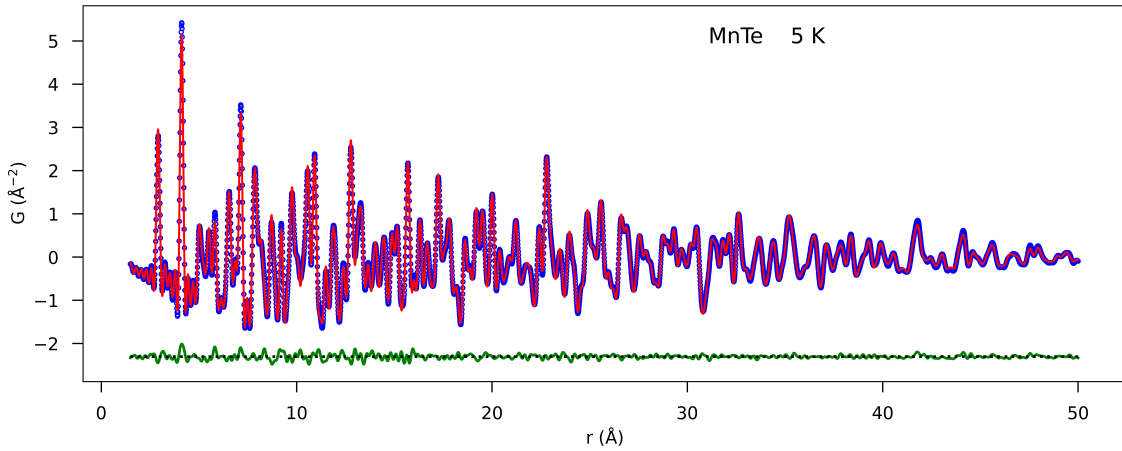


FIG. S1. X-ray PDF fit for pure MnTe at 5 K. The blue symbols represent the experimental data, the red curve the best-fit calculated PDF, and the green curve the fit residual, offset vertically for clarity.

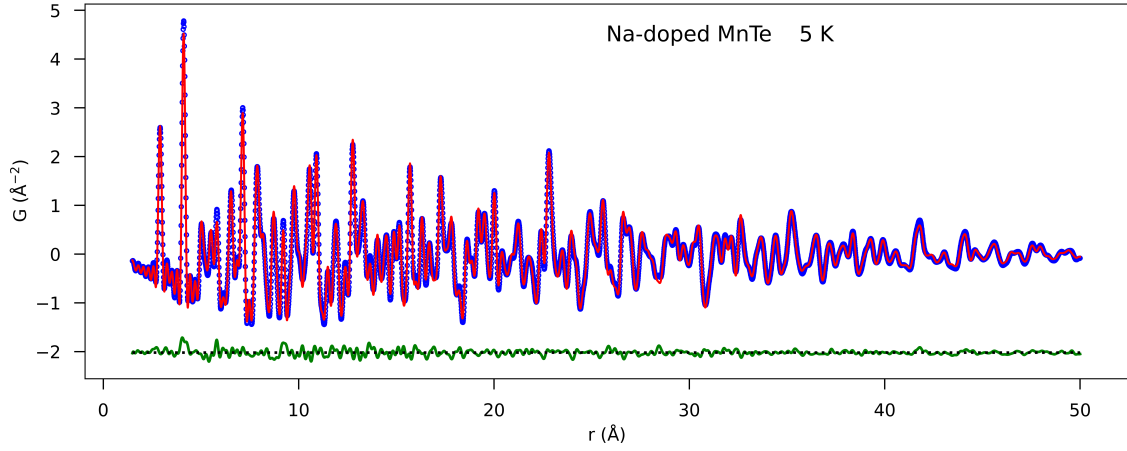


FIG. S2. X-ray PDF fit for MnTe doped with 2% Na at 5 K. The blue symbols represent the experimental data, the red curve the best-fit calculated PDF, and the green curve the fit residual, offset vertically for clarity.

The Supplemental Information includes additional details and data regarding the PDF fits, the Debye-Grüneisen modeling of the lattice parameters and unit cell volume, the linear scaling between the lattice response and the local magnetic order parameter, the PDF measurements with an *in situ* magnetic field, and the magnetic domain structure and associated free-energy arguments for Na-doped MnTe.

Representative PDF fits. Representative fits to the x-ray PDF data collected at 5 K using the published hexagonal structure for MnTe are shown for pure MnTe in Fig. S1 and for Na-doped MnTe in Fig. S2. The fit quality is good in both cases, indicating that the published structure provides a good model for the data. Equivalent fits were conducted for all data sets collected between 5 and 500 K.

Debye-Grüneisen fits. The best-fit parameter values for the Debye-Grüneisen fits to the lattice parameters and unit cell volume for pure and doped MnTe are given in Table I. The values for $\frac{\gamma}{B_0}$ are similar but not identical for the fits performed against the volume, a lattice parameter, and c lattice parameter. The differences reflect anisotropies in the elastic properties of the solid. Using the volume result for pure MnTe and substituting in the reported bulk modulus of 47.3 GPa [1], we can estimate the Grüneisen parameter to be $\gamma = 1.6$, a reasonable value for solids that supports the reliability of this approach. The values of γ/B_0 are also close to those reported for other binary antiferromagnetic compounds [2, 3].

The Debye-Grüneisen fits to the lattice parameters for Na-doped MnTe are shown in Fig. S3. We used a Debye temperature of 223 K, which was also used for pure MnTe. The measured

TABLE I. Best-fit parameter values from Debye-Grüneisen fits to the lattice parameter data for pure and doped MnTe.

	V_0 (Å ³) or ℓ_0 (Å)	γ/B_0 (Pa ⁻¹)
MnTe		
Volume fits	98.947(8)	$3.42(1) \times 10^{-11}$
a parameter fits	4.137(1)	$2.0(4) \times 10^{-11}$
c parameter fits	6.6798(3)	$1.40(1) \times 10^{-10}$
Na-doped MnTe		
Volume fits	99.06(1)	$3.35(2) \times 10^{-11}$
a parameter fits	4.1358(3)	$2.10(8) \times 10^{-11}$
c parameter fits	6.6906(5)	$1.27(2) \times 10^{-10}$

unit cell volume as a function of temperature for both compounds is plotted in Fig. S4, together with the predicted temperature dependence based on the Debye-Grüneisen model. The pure and doped compounds both show nearly indistinguishable trends. At the lowest temperature, $\Delta V/V$ is -7.3×10^{-3} for pure MnTe and -7.8×10^{-3} for Na-doped MnTe.

Linear scaling of the lattice response with the local magnetic order parameter. In Fig. S5, we plot the fractional lattice change versus the local magnetic order parameter (LMOP) for the a and c lattice parameters of pure MnTe as well as a , c , and the unit cell volume for Na-doped MnTe. In all cases, a predominantly linear relationship is clearly observed.

Field-dependent PDF measurements. To investigate the possibility of forced magnetostriction in MnTe, we performed x-ray PDF measurements with an *in situ* magnetic field up to 5 T. Data were collected for pure MnTe at temperatures of 24 K, 290 K, 350 K, and 400 K. No field-induced change is observed in the individual lattice parameters or the unit cell volume at any temperature, as illustrated in Fig. S6. We can estimate a generous upper limit of the forced volumetric magnetostriction in MnTe in fields up to 5 T by considering the difference between the maximum volume plus one estimated standard deviation (ESD) and the minimum volume minus one ESD. The largest upper limit estimated in this way is $\Delta V/V = 6.3 \times 10^{-4}$. An upper limit that is perhaps more

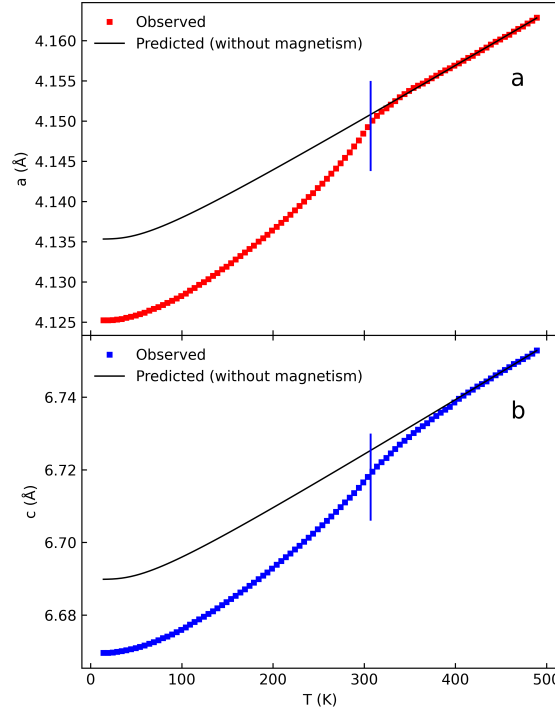


FIG. S3. Temperature dependence of the a (panel a) and c (panel b) lattice parameters for Na-doped MnTe determined from x-ray PDF fits. The solid black curve shows the prediction using the Debye-Grüneisen model, which does not take into account magnetostructural effects.

realistic can be obtained by fitting a line or parabola to the data points and calculating the largest magnitude of $\Delta V/V$ from the fitted curve. This largest upper limit produced by this procedure is 1.5×10^{-4} for 290 K.

Magnetic domain coupling for Na-doped MnTe. Lightly doping MnTe with Na or Li causes a reorientation of the spins such that they lie nearly along the c axis at low temperature, gradually canting further away from the c axis toward the in-plane spin arrangement in pure MnTe as the temperature is increased toward the transition [4, 5]. Given the small energy difference between the in-plane and out-of-plane spin arrangements, it is reasonable to expect that the short-range correlations in the paramagnetic state may also include out-of-plane components. The out-of-plane spin component corresponds to the one-dimensional Γ_4^+ irreducible representation of space group $P6_3/mmc$ (#194), which permits two domains corresponding to opposite orientations relative to the c axis. Combining two out-of-plane domains with six in-plane domains results in a set of 12 joint order parameter (OP) domains. Regardless of the number of domains, the fundamental idea is the same, namely that the long-range OP in the reference domain arises at T_N , while the short-range OP in other domains pre-exists at T_N . When they are coupled, approximately linear scaling arises,

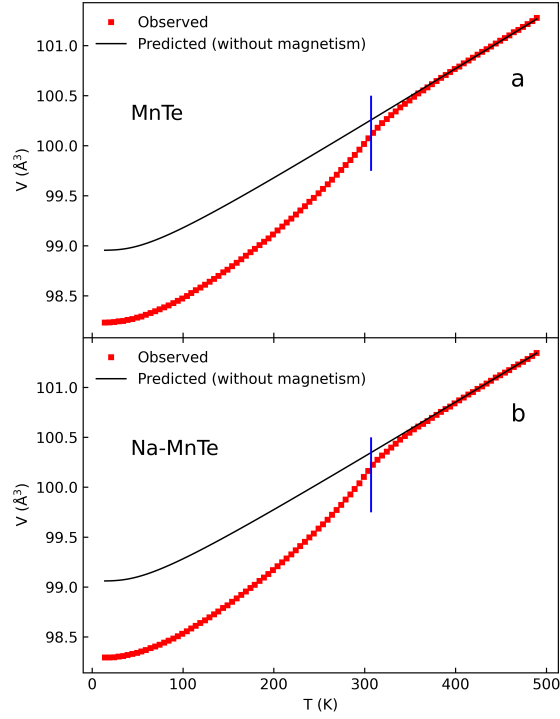


FIG. S4. Temperature dependence of the unit cell volume for pure MnTe (a) and Na-doped MnTe (b) determined from x-ray PDF fits. The solid black curves show the prediction using the Debye-Grüneisen model, which does not take into account magnetostructural effects.

as explained in the main text.

-
- [1] W. Paszkowicz and E. Dynowska, HIGH PRESSURE - HIGH TEMPERATURE DIFFRACTION STUDY OF MnTe USING SYNCHROTRON RADIATION, *Acta Phys. Pol. A* **91**, 939 (1997).
 - [2] T. Chatterji, G. N. Iles, B. Ouladdiaf, and T. C. Hansen, Magnetoelastic effect in MF_2 ($M = \text{Mn, Fe, Ni}$) investigated by neutron powder diffraction, *J. Phys.: Condens. Mat.* **22**, 316001 (2010).
 - [3] T. Chatterji and T. C. Hansen, Magnetoelastic effects in Jahn–Teller distorted CrF_2 and CuF_2 studied by neutron powder diffraction, *J. Phys.: Condens. Mat.* **23**, 276007 (2011).
 - [4] D. H. Moseley, K. M. Taddei, J. Yan, M. A. McGuire, S. Calder, M. M. H. Polash, D. Vashaee, X. Zhang, H. Zhao, D. S. Parker, R. S. Fishman, and R. P. Hermann, Giant doping response of magnetic anisotropy in MnTe, *Phys. Rev. Materials* **6**, 014404 (2022).
 - [5] R. Baral, J. Christensen, P. Hamilton, F. Ye, K. Chesnel, T. D. Sparks, R. Ward, J. Yan, M. A. McGuire, M. E. Manley, J. B. Staunton, R. P. Hermann, and B. A. Frandsen, Real-space visualization

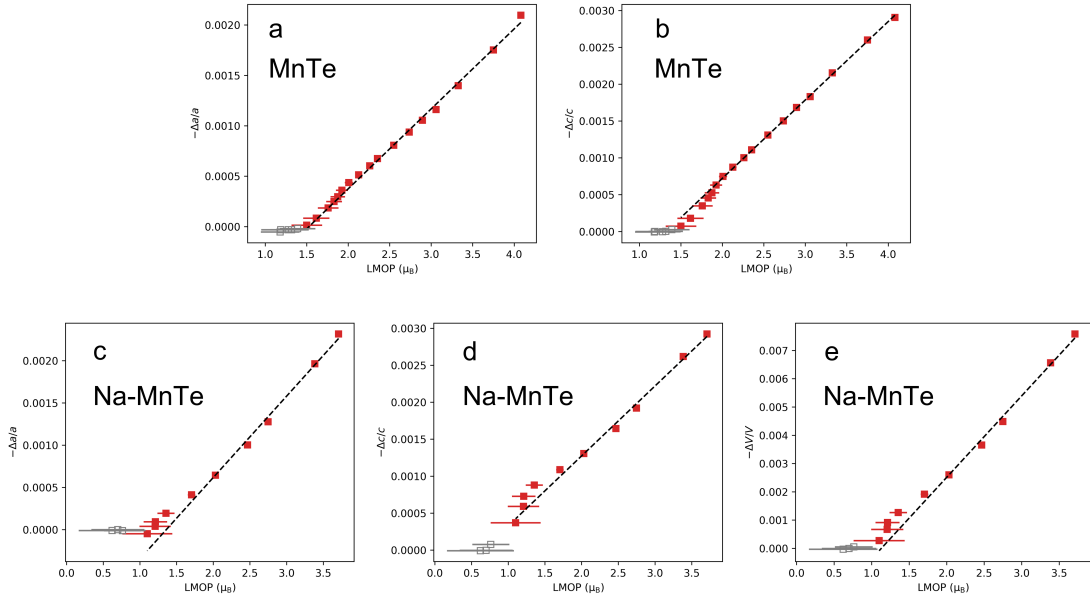


FIG. S5. (a, b) The fractional change in a (panel a) and c (panel b) versus the LMOP in pure MnTe. The black dashed line is a best-fit line to the red data points. The gray data points were left out of the fit because they represent data collected at high temperatures above the onset of the magnetostructural response. (c-e) Same as (a, b) but for Na-doped MnTe and with the fractional volume shift included as panel (e).

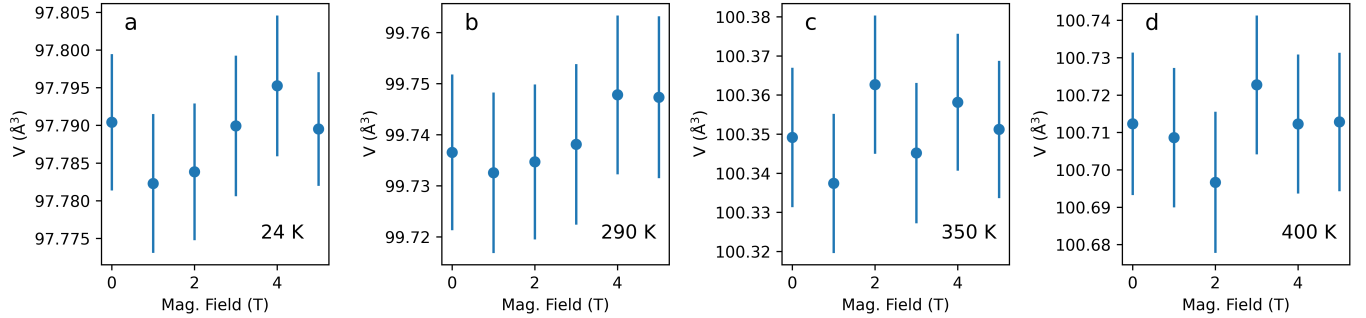


FIG. S6. Unit cell volume versus applied magnetic field for pure MnTe at 24 K (a), 290 K (b), 350 K (c), and 400 K (d). The error bars represent the estimated standard deviation.

of short-range antiferromagnetic correlations in a magnetically enhanced thermoelectric, *Matter* **5**, 1853 (2022).